Nanotechnology

Enhanced magnetism derived from pore-edge spins in thin Fe_3GeTe_2 nanomeshes

To cite this article before publication: Reiji Obata *et al* 2024 *Nanotechnology* in press https://doi.org/10.1088/1361-6528/ad6fa2

Enhanced magnetism derived from pore-edge spins in thin Fe_3GeTe_2 nanomeshes

R. Obata[1], M. Kosugi[1], Y. Oguchi[1], H. Sun[2], T. Kikkawa[3], C. Tomatsu[1], K. Suenaga[2], E. Saitoh[3,6-8], S. Maruyama[4], J. Haruyama[1,5,*]

[1]*Faculty of Science and Engineering, Aoyama Gakuin University, 5-10-1 Fuchinobe, Sagamihara, Kanagawa 252-5258, Japan*
[2]*The Institute of Scientific and Industrial Research, Osaka University Mihogaoka 8-1, Ibaraki, Osaka 567-0047, Japan*
[3]*Department of Applied Physics, The University of Tokyo, 7-3-1 Hongo, Bunkyo-ku, Tokyo 113-8656, Japan*
[4]*Department of Mechanical Engineering, The University of Tokyo, 7-3-1 Hongo, Bunkyo-ku, Tokyo 113-8656, Japan*
[5]*Institute for Industrial Sciences, The University of Tokyo, 4-6-1 Komaba Meguro-ku, Tokyo 153-8505, Japan*
[6]*Institute for AI and Beyond, The University of Tokyo, 7-3-1 Hongo, Bunkyo-ku, Tokyo 113-8656, Japan*
[7]*WPI Advanced Institute for Materials Research, Tohoku University, 2-1-1 Katahira, Aoba-ku, Sendai 980-8577, Japan*
[8]*Advanced Science Research Center, Japan Atomic Energy Agency, 2-4 Shirakata, Tokai-mura, Naka-gun, Ibaraki 319-1195, Japan*

* J-haru@ee.aoyama.ac.jp

Abstract. The growth of two-dimensional (2D) van der Waals (vdW) magnetic materials presents attractive opportunities for exploring new physical phenomena and valuable applications. Among these materials, Fe_3GeTe_2 (FGT) exhibits a variety of remarkable properties and has garnered significant attention. Herein, we have for the first time created a nanomesh structure—a honeycomb-like array of hexagonal nanopores—with the zigzag pore-edge atomic structure on thin FGT flakes with and without oxidation of the pore edges. It is revealed that the magnitude of ferromagnetism (FM) significantly increases in both samples compared with bulk flakes without nanomeshes. Critical temperature annealing results in the formation of zigzag pore edges and interpore zigzag-edge nanoribbons. We unveil that the non-oxide (O) termination of the Fe dangling bonds on these zigzag edges enhances FM behavior, while O-termination suppresses this FM by introducing antiferromagnetic behavior (AFM) through edge O-Fe coupling. FGT nanomeshes hold promise for the creation of strong FM and their effective application in magnetic and spintronic systems.

Keywords: van der Waals magnetic materials, magnetism, edge, nanopores, nanoribbons, oxidation

1.Introduction

The emergence of two-dimensional (2D) van der Waals (vdW) materials has led to the discovery of novel physical phenomena and applications in various devices and systems. In particular, realizing room-temperature long-range spin ordering in 2D thin materials is a key to create flexible magnetic and spintronic-devices. High electronic density of states (*i.e.*, edge states) originating from flat energy band of zigzag-type atomic structure of graphene nanoribbon (GNR) edges and subsequently the appearance of flat-band ferromagnetism (FM) were theoretically predicted and confirmed experimentally in H-terminated zigzag-edged GNRs and also our graphene nanomeshes (GNMs), consisting of a honeycomb-like array of hexagonal nano-pores fabricated using a non-lithographic method [1,2]. Because a GNM corresponds to a large ensemble of GNRs (i.e., interpore narrow regions), it is very effective to detect small magnetic signals arising from the pore edge spins. We have also yielded magnetism and spin-based phenomena arising from pore edge spins in other various nanomeshes created on various 2D thin layers [3-6]; *e.g.*, black phosphorus [3], hexagonal boron nitride (hBN) [4], molybdenum di-sulfide (MoS_2) [5], bismuth telluride (Bi_2Te_3) [6]. Each individual nanomesh exhibits intriguing magnetic phenomena originating from the electronic and spin states at the pore edges.

In conventional 2D materials, the edge volume is typically very small, as it exists solely along the edges of a sample. Furthermore, edges are often plagued by numerous defects and contamination. These factors have made it challenging to detect the magnetism arising from edge spins. Our 2D thin nanomesh structure resolves this problem by virtue of fewer defects and less contamination at the pore edges, because it is fabricated by using a nonlithographic fabrication method, which involves etching 2D thin layers using a nanoporous alumina template (NPAT) mask and low-power Ar gas. The large-volume dangling bonds present at the nanopore edges of the zigzag atomic structure (*e.g.*, with a pore diameter ~ 50 nm and a pore density ~ $10^{11}/cm^2$) with less-defects and - contamination in the 2D nanomeshes enabled the straightforward observation of edge-derived magnetism, depending on the materials and the foreign atoms terminating the zigzag pore edges (*e.g.*, O and hydrogen).

On the other hand, a magnetic layer, Fe_3GeTe_2 (FGT), has recently taken center stage in magnetic material research due to its remarkable magnetic and spintronics properties. FGT exhibits various attractive features, *e.g.*, gate-tunable high Currie temperature (*e.g.*, $T_c \simeq$ 230 K) depending on thickness (even extend up to 300 K) [8-12], interlayer-coupling based magnetisms [13], and Néel-type magnetic skyrmions in the FGT/[Co/Pd] multilayers or oxidized(O)-FGT at zero magnetic field [14-16]. Furthermore, FGT layers have been revealed worth as electrodes or barriers in vdW magnetic tunnel junctions (MTJs) and giant magnetoresistance (GMR) devices [17-20].

However, the electronic and magnetic properties of FGT remain enigmatic. The atomic and lattice structures of FGT are intricate (see figure 1(a,b)), and various theoretical reports have proposed different electronic and magnetic (spintronic) states. These variations depend on the positions of the Ge, Te, and two Fe atoms, as well as intralayer and interlayer interactions [21-24]. O-termination and strain also play significant roles in influencing these states. Especially, influence of edge spins has been merely observed.

The primary magnetic behavior of FGT is FM. In contrast, the emergence of both FM and anti-ferromagnetism (AFM) is highly sensitive to the direct exchange interaction among Fe_{1-3} atoms and the superexchange interaction among Fe_{1-3}, Te, and Ge atoms [21]. The distances (d_s) and angles (θ) among atom sites (figure 5(c)) can be modulated by strain or other factors, resulting in significant changes in the observed magnetism. Following this, experiments involving strain applied to FGT showed that increasing θ and d_s can yield a higher FM magnitude [21]. Conversely, when two FGT layers are directly vdW integrated, the strong intraplane exchange interaction among Fe_{1-3} atoms

resulted in AFM spin alignments [24]. In the surface O-FGT layer, the *p*-orbital AFM spin of O atoms could couple with the bulk FM layers through Fe_3 - Ge superexchange interactions and mediated, depending on the O-terminated sites [25].

In the present study, we have created the nanomesh structure on thin 2D FGT flakes in order to clarify influence of edge spins to magnetic and spintronic of FGTs. The unique atomic structure of FGT results in two distinct types of zigzag pore edges, with $Fe_{1\text{-}3}$ atoms forming dangling bonds and, as a consequence, interpore nanoribbon regions with the zigzag edges. It is revealed that the absence of O-termination on these $Fe_{1\text{-}3}$ dangling bonds drastically enhances the FM magnitude of the FGT nanomesh, whereas the O-termination suppresses this FM behavior by potentially introducing AFM.

2.Results and discussion

2.1 Sample fabrication and characterization

Thin FGT flakes are obtained through the mechanical exfoliation of bulk samples using the Scotch tape method. Multiple flakes were found on a SiO_2/Si substrate (*e.g.*, an area measuring a few ~ 100 μm^2 and a thickness ranging from ~ 10 – ~ 60 nm). The thicker flakes (>> 30 nm) are mechanically removed. An example of planer (c) and cross-sectional (d) atomic force microscope images for a typical FGT flake used in nanomesh formation is shown in figure 1(c, d). Examples of Electron energy loss spectroscopy (EELS) elemental mapping and X-ray photo spectroscopy (XPS) measurement are presented in figures 1(f) and 1(g), respectively. Each element (Fe, Ge, Te) is certainly confirmed in these figures. The large peaks with the binding energies ~720 eV and ~707 eV for $Fe2p_{1/2}$ and $Fe2p_{3/2}$, ~30 eV for Ge3d, and ~584 eV and ~573 eV for $Te3d_{3/2}$ and $Te3d_{5/2}$ are evidently observed for XPS spectrum, respectively. Moreover, a very small peak is also confirmed at ~577 eV for $Te3d_{5/2}$.

The NPAT masks are formed through self-organization by anodic alumina oxidation (AAO) of pure aluminum substrates (99.9999%) using $C_2H_2O_4$ solution, following our established method [15-20]. An example of scanning electron microscopy (SEM) image of the NPAT mask is shown in figure 2(a), which presents mean pore diameters ~60 nm and mean interpore distances ~20 nm with high regularity.

Procedure for the FGT nanomesh fabrication is presented in figure 2. The NPAT masks are placed on substrates, including the abovementioned FGT flakes, and the nanopore array is then transferred to the FGT flakes using careful low-power Ar gas etching avoiding introduction of damages and contamination on the pore edges. An example atomic force microscopy (AFMS) image of the resulting FGT nanomesh formed by this method is shown in figure 3(b), displaying mean pore diameters ~60 nm and mean interpore distances (*d*) of ~20 nm, which are almost the same as those in the NPAT mask. The nanomeshes are subsequently annealed in a high vacuum environment (10^{-6} Torr) at an optimized high-temperature (700 °C), because this annealing results in the most stable structure with respect to chemical and thermal conditions, which can be a zigzag atomic structure following our past obtaining for the various nanomeshes as explained in latter part (figures 5(b,d)) [15-20].

Indeed, the higher-resolution images of one pore (figures 3(c) and 3(d)) reveals possible formation of the zigzag pore edges. The corner of pore edge and other irregular edge parts can exactly correspond to the angle ~120° (as fit by dotted hexagons in figure 3(d)). Such edge angles result in the zigzag atomic structure from topological reason (see figure 6(a)). Then, one sample is used for magnetization measurement without pore oxidation, while the other is exposed to the ambient air atmosphere for 5 hours to establish O-terminated pore edges (*i.e.*, the O-nanomesh). Non-degradation of the O-nanomesh sample after this oxidation process is confirmed by observation of EELS spectrum. Moreover, the large magnetization values observed for the O-nanomesh mentioned in later (table 2) reconfirmes non-degradation of the samples.

Si substrates with the FGT nanomeshes on the surface are collected (*e.g.*, total area < ~1×5 mm^2)

and then positioned inside a tube within a superconducting quantum interference device (Quantum Design; MPMS), allowing the magnetic behavior of the material to be measured by applying an in-plane magnetic field. An example of magnetization curve on temperature change is shown in figure 1(e). It suggests (onset) $T_c \simeq 250$ K, which is almost consistent with previous reports for thickness ~25 nm.

2.2 Magnetic properties

Examples of the magnetization curves of the non-O-terminated nanomesh, O-terminated nanomesh, and exfoliated pristine thin bulk flake are demonstrated in figure 4. The summary of the magnetization values and coercivity for each sample are also provided in table 1. Magnetization values are normalized by mass based on the sample area without considering the presence of nanopores in the naomeshes as following. The size of unit cell of FGT is ~0.3nm x 0.3nm x 2nm and the flake size is ~100um x 100um x 0.1um. Thus, number of $\sim 6 \times 10^{13}$ unit cells are included in the flakes. Mass/mol(6×10^{23} atoms) for Fe, Ge, and Te are 56g/mol, 73g/mol, and 128g/mol, respectively. Hence, the total mass of $\sim 400 \times 10^{-10}$ g of atoms are included in a unit cell (with three Fe atoms, one Ge, and one Te atom), based on number of $\sim 6 \times 10^{13}$ unit cells/flake. Consequently, a magnetization unit of 1×10^{-6} emu/area corresponds to 2.5 emu/g.

All samples present ferromagnetic curves. Exfoliated pristine thin FGT flakes (*i.e.*, without nanomesh) show only small-magnitude of the FM with the very small saturation and residual magnetization values (M_s and M_r, respectively) and coercivity (figure 4(c) and table 1).

In contrast, both the non-O-terminated nanomesh and O-terminated nanomesh exhibit considerably larger-magnitude of the FM; significantly larger values for M_s, M_r, and coercivity, approximately 10 ~ 17 times, 10 ~ 13 times, and ~1.7 times larger, respectively (figure 4(a,b)), compared with the thin bulk flake (figure 4(c)) (table 1). The values in the O-terminated nanomeshes are considerably larger than those in the non-nanomesh samples in previous reports (table 2) [8-12], emphasizing robust influence of the pore-edge spins. It is more striking that the M_s and M_r of the non-O-terminated nanomesh (figure 4(a)) are ~1.7-times larger than those of the O-terminated nanomesh (figure 4(b)) (table 1).

The dependence of magnetic curves (M_s and M_r values) on the mean d for the non-O-terminated nanomeshes with annealing temperature (T_a) of 700 °C is shown in figures 5(a) and 5(c). Magnitude of the FM becomes considerably larger as d decreases (figure 5(a)). M_s and M_r values also greatly increase with decreasing d (figure 5(c)). T_a dependence of magnetic curves for the non-O nanomesh with d = 20nm is exhibited in figures 5(b) and 5(d). The strongest FM curve with the largest M_s and M_r values are observed at $T_a \sim 700$ °C, which is close to the growth temperature of the bulk FGT crystal. Based on this result, this T_a(= 700 °C)-annealing has been employed for all other samples in the present experiments.

2.3 Discussion

As a result, we have observed the emergence of significantly large magnetism in FGT nanomeshes. We provide a qualitative discussion of the factors contributing to these magnetisms. The dependence on d and T_a for magnetism is similar to what we observed in our previous various 2D nanomeshes with zigzag atomic-structure pore edges [1-6], corresponding to the zigzag-edge nanoribbons in the interpore regions, as mentioned below.

Concerning T_a, it's well known that zigzag-edge atomic structure of nanoribbons (*i.e.*, interpore regions) is highly sensitive to chemical and thermal conditions. When nanomesh samples are annealed at a critical temperature which close to the growth temperature of bulk crystals, reconstruction of the

edge atomic structure occurs, resulting in formation of the zigzag atomic structure with the highest magnetization value because the zigzag edge structure is the most stable from chemical and thermal viewpoints.

In contrast, even very small shift from the critical condition leads to destruction (or disorder) of the zigzag structure, resulting in a decrease in magnetization. The $T_a \sim \sim 700$ °C can correspond to this critical condition, because that is close to the growth temperature of the current bulk FGT and the magnetization values decrease by annealing at 600 °C and 800 °C.

Moreover, our previous research on various-2D material nanomeshes [1-6] also supports this argument, because each nanomesh provided such critical T_a at which the highest M_s value appears, resulting in the zigzag pore edges. This annealing process at 700 °C also effectively eliminates defects and contamination at the pore edges, avoiding an increase in magnitude of the FM originating from such defects.

This discussion implies that the present FGT nanomeshes possess a similar zigzag pore-edge (*i.e.*, zigzag edges of the interpore nanoribbon region) structure as shown in figures 3(d) and 6(a,b). When hexagonal nanopores are introduced onto the FGT lattice structure, two distinct types of zigzag pore edges emerge with $Fe_{1,3}$ or Fe_2 atom dangling bonds (figure 6(a)). This leads to the formation of nanoribbons situated between these two different zigzag pore edges within the interpore region (figure 6(a,b)).

The primary magnetic structure of FGTs is FM, while the presence of AFM has been both theoretically and experimentally reported as mentioned in the introduction. One of the most plausible theoretical explanations for this is presented in *ref*. 21 as follows. The stability of FM coupling can be understood through the Goodenough−Kanamori−Anderson rules. The magnetic ground state of the FGT monolayer is determined by the competition between the direct exchange interaction and the superexchange interaction. In the case of the direct exchange interaction, the *d* orbitals on the nearest-neighbor Fe atoms overlap directly, without a mediation atom. This yields AFM coupling, which is determined by the distance between the neighboring Fe atoms. On the other hand, in the superexchange interaction, the *d* orbitals on the nearest-neighbor Fe atoms overlap with the *p* orbitals of Ge or Te atoms. Consequently, the superexchange mediated by Ge or Te atoms causes FM coupling. The strength of FM coupling is principally sensitive to the Fe−Te (Ge)− Fe angle (θ) and those distance (d_s) (figure 6(c)). If the superexchange interaction overcomes the direct exchange interaction, FGT exhibits FM coupling, otherwise AFM coupling emerges. This interpretation was evidenced by experiments applying strain to FGTs, which allowed the control of θ and d_s [21]. When $\theta_{1,2}$ and $d_{s1,2}$ increased due to applied strain, the magnitude of FM actually increased.

In this context, one can qualitatively understand the significant enhancement of FM in the current non-Oxygen nanomesh from this model. When zigzag edges of the interpore nanoribbons are formed (figure 6(a,b)), dangling bonds consisting of Fe_1, Fe_3, and Fe_2 atoms at the edges, along with neighboring atoms, experience more significant relaxation compared to the bulk regions. This is because they have more freedom at the pore edges. This increased relaxation qualitatively leads to an increase in parameters θ and d_s, (e.g., $\theta_{1,2}$ and $ds_{1,2}$ at points B and A, respectively) (figure 6(c)) and induce the FM magnitude. The M_s and M_r values of the non-O nanomeshes monotonically increased with decreasing *d*. This result reinforces the argument, because the FM spin alignment between both edges of the interpore nanoribbon region is enhanced with decreasing *d* as observed in previous reports [1-6], while AFM spin alignment remains independent of *d*. Moreover, when presence of the nano pores is considered for the normalization of magnetization values with mass, the M_s and M_r values of the non-O nanomeshes are estimated to become ~100-time greater than those in thin bulk samples without the nano pores (based on the radius ratio for pore (~30nm) and cell (~40nm)). Because such

huge M values cannot be understood by uniform distribution of the FM spins to the narrow interpore regions, those localization on the relaxed dangling bonds consisting of Fe_1, Fe_3, and Fe_2 atoms at the zigzag pore edges is indispensable.

In contrast, the O-termination of nanomeshes reduces the values of M_s and M_r to approximately half values. This difference can be attributed to the presence of AFM, which arises from the coupling between edge Fe and O atoms (figure 6(d)). This is because, conventionally, the O-termination of Fe atoms at the dangling bonds suppresses FM spin alignment, inducing AFM spin coupling, as previously mentioned [24,25]. Nevertheless, substantial FM still persists in the O-nanomesh, resulting in the small difference as mentioned above. This resilience may be due to spin splitting in the Te3$d_{5/2}$ orbital, resulting from strong Te-O coupling at the edge dangling bonds, and the consequent induction of FM spin alignment (figure 6(d)), as we previously reported in the context of FM for the Bi_2Te_3 nanomesh [6]. Moreover, it was reported that the boundary (interface) between O-AFM and non-O FM regions may lead to an increase in Neel skyrmion creation [25]. This observation may correspond to the interplay of edge O-AFM and non-O FM within the nanoribbon regions, potentially contributing to the persistence of substantial FM.

3. Conclusion

In conclusion, we fabricated a nanomesh structure (a honeycomb-like array of hexagonal nanopores) with the zigzag pore-edge atomic structure, which was possibly reconfirmed by the high-resolution AFMS images, on thin FGT flakes with and without oxidation of the pore edges. Notably, our findings revealed a significant increase in the magnitude of FM in both samples when compared to bulk FGT flakes lacking the nanomesh structure. The critical temperature annealing resulted in formation of the zigzag pore edges, corresponding to creation of the interpore zigzag-edge nanoribbons regions which considerably contributed to this drastic FM enhancement. It was revealed that the non-O termination of the $Fe_{1\text{-}3}$ dangling bonds of these zigzag edges drastically enhanced FM behaviors due to possible increase in θ and d_s by an increase in the lattice freedom at the pore edges, while the O-termination suppressed this FM by introducing AFM through edge O - $Fe_{1\text{-}3}$ coupling. Moreover, investigation of the contribution of magnetic Skirmion unique to FGTs is expected for the observed drastic enhancement of the FM. The FGT nanomeshes hold promise for generating significant magnetism and have potential applications in the field of magnetic and spintronic devices.

Acknowledgements

We thank K. Nomura, T. Koretsune, K. Otsuka, K. Hirakawa, T. Ando, A. H. Macdonald, C. Lee, J.J. Palacios, R. Wu, and P. Kim for their technical contributions, fruitful discussions, and encouragement. The work at the Aoyama Gakuin University was partly supported by the Aoyama Gakuin University Research Institute grant program for the creation of innovative research. Work at the University of Tokyo was partly supported by JSPS KAKENHI (Grant Numbers JP23H00174, JP23H05443) and by JST, CREST (Grant Number JPMJCR20B5, Japan) for S.M. and JST-CREST (JPMJCR20C1 and JPMJCR20T2), Grant-in-Aid for Scientific Research (JP19H05600 and JP22K18686) and Grant-in-Aid for Transformative Research Areas (JP22H05114) from JSPS KAKENHI, MEXT Initiative to Establish Next-generation Novel Integrated Circuits Centers (X-NICS) (JPJ011438), Japan, and Institute for AI and Beyond of the University of Tokyo for T. K. and E. S..

Data availability statement

All data that support the findings of this study are included within the article.

References

[1] J. Haruyama, Special Issue on “Carbon Nanoelectronics" in *Electronics*, **2**, 368 (2013).

[2] T. Hashimoto, J. Haruyama, D. Soriano, S. Roche, *Appl. Phys. Lett.* **105**, 183111 (2014).

[3] Y. Nakanishi1, A. Ishi, C. Ohata, D. Soriano, R. Iwaki, K. Nomura, M. Hasegawa, T. Nakamura, S. Katsumoto, S. Roche, *Nano Research* **10,** 718 (2017).

[4] C. Ohata, R. Tagami, Y. Nakanishi, R. Iwaki, K. Nomura, J. Haruyama, *Appl. Phys. Lett.* **109**, 133110 (2016).

[5] G. Kondo, N. Yokoyama, S. Yamada, Y. Hashimoto, C. Ohata, S. Katsumoto, and J. Haruyama, *AIP Advances* **7**, 125019 (2017)

[6] T. Kobayashi, H. Mine, T. Tokuda, Y. Hashimoto, S. Katsumoto, and J. Haruyama, *Appl. Phys. Lett.* **115**, 093101 (2019).

[7] Y. Deng, Y. Yu, MZ. Shi *et al.*, *Nature* **563**, 94 (2018).

[8] F. May, D. Ovchinnikov, Qi. Zheng, R.Hermann, S. Calder, B. Huang, Z. Fei, Y. Liu, X. Xu, and M. A. McGuire, *ACS Nano* **13**, 4436 (2019).

[9] C. Zhang et al., *Nature Commun.* **15**, 4472 (2024).

[10] K. Kim *et al., Nature Mat*. **17**, 794 (2018).

[11] M. Wang *et al., npj 2D Materials and Applications* **8**, 22 (2024).

[12] H. Wang *et al., Appl. Phys. Lett.* **116**, 192403 (2020).

[13] H. K. Gweon, S. Y. Lee, H. Y. Kwon *et al., Nano Lett*. **21**, 1672 (2021).

[14] M. Yang, Q. Li, R. V. Chopdekar *et al., Sci. Adv*. **6**, eabb5157 (2020).

[15] Y. Wu, S. Zhang, J. Zhang*et al., Nature Commun.***11**, 3860 (2020).

[16] B. Ding, X. Li, Z. Li, X. Xi, Y. Yao and W. Wang, *NPG Asia Materials* **14**, 74 (2022).

[17] Z. Wang, D. Sapkota, T. Taniguchi, K. Watanabe, D. Mandrus, and A. F. Morpurgo, *Nano Lett.* **18**, 4303 (2018).

[18] S. Albarakati, C. Tan, Z.-J. Chen *et al., Sci. Adv*. **5**, eaaw0409 (2019).

[19] H. Lin, F. Yan, C. Hu, Q. Lv, W. Zhu, Z. Wang, Z. Wei, K. Chang, and K. Wang, *ACS Appl. Mater. Interfaces* **12**, 43921 (2020).

[20] R. Obata, H. Sun, K. Samanta, M. Kosugi, T. Kikkawa, T. Taniguchi, K. Watanabe, K. Suenaga, E. Saitoh, S. Maruyama, K. Hirakawa, K. D. Belashchenko, E. Y. TsymbalJ. Haruyama Submitted to *Nano Letters*

[21] X. Hu, Y. Zhao, X. Shen, A. V. Krasheninnikov, Z. Chen, and L. Sun, *ACS Appl. Mater. Interfaces* **12**, 26367 (2020).

[22] J. Yi, H. Zhuang, Q. Zou, Z. Wu, G. Cao, S. Tang, S. A. Calderc , P. R. C. Kent, D. Mandrus, and Z. Gai, *2D Mater*. **4**, 011005 (2017).

[23] Z.-X. Shen, X. Bo, K. Cao, X. Wan, and L. He, *Phys. Rev*. **B** 103, 085102 (2021).

[24] D. Kim, S. Park, J. Lee *et al., Nanotechnology* **30**, 245701 (2019).

[25] Y. Li, X. Hu, A. Fereidouni *et al., ACS Appl. Nano Mater.* **6**, 4390 (2023).

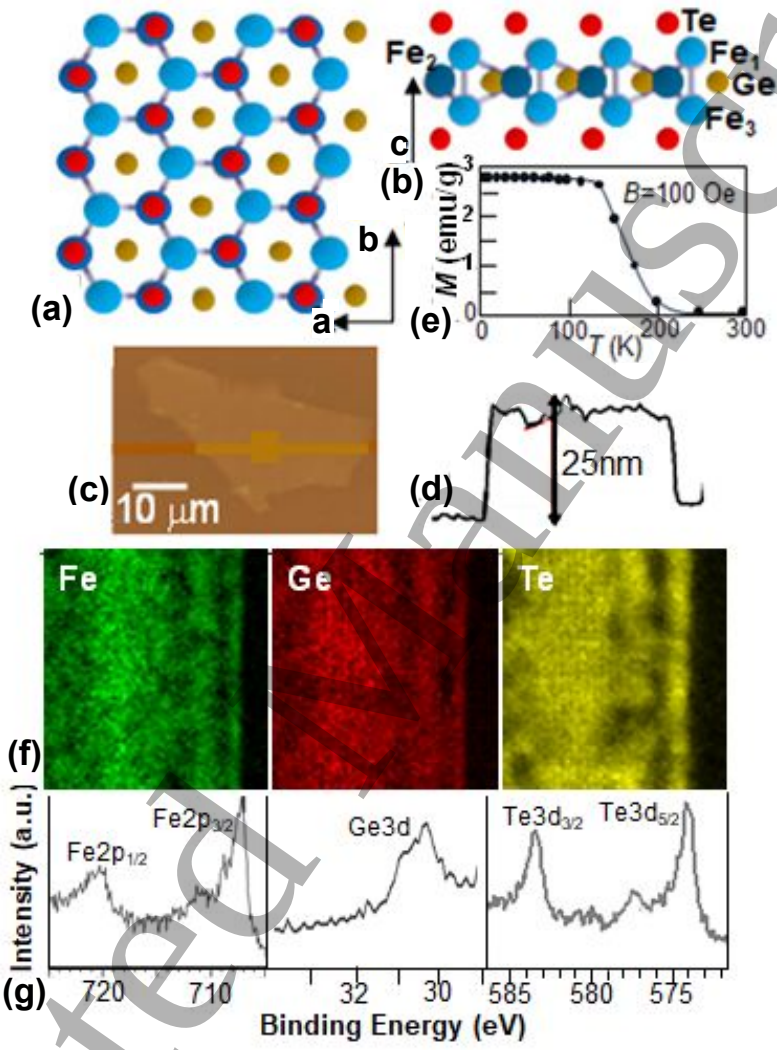

Figure 1. Schematic views of the atomic structure of FGT for **(a) the** x-y plane and **(b)** the z direction. Examples of **(c)** optical and **(d)** cross-sectional atomic force microscope images for an FGT flake. **(e)** An example of magnetization curve on temperature change. **(f,g)** Examples of EELS mapping for each element **(f)** and XPS measurement **(g)**.

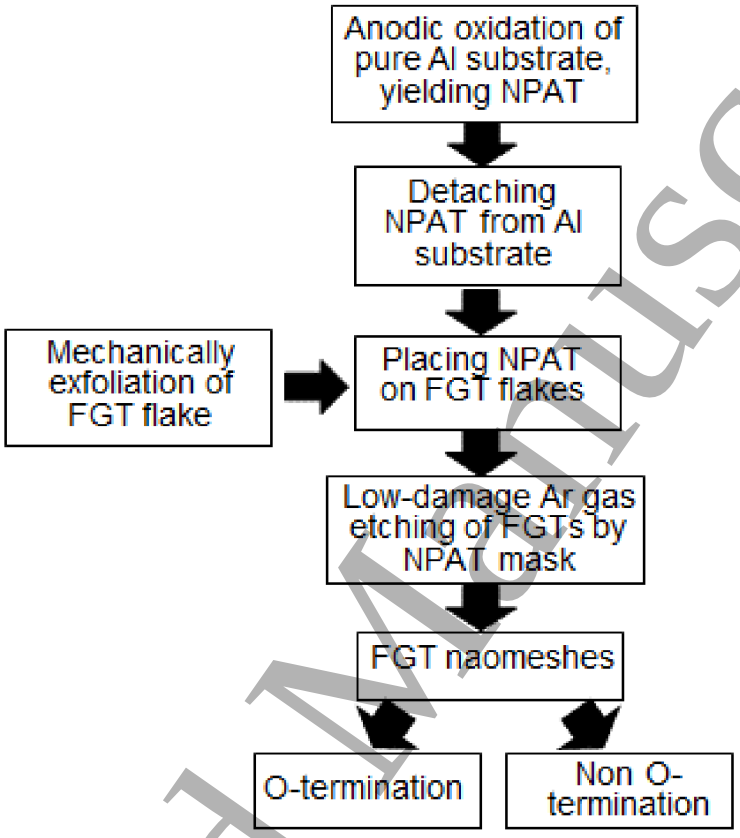

Figure 2. Sample preparation flow chart.

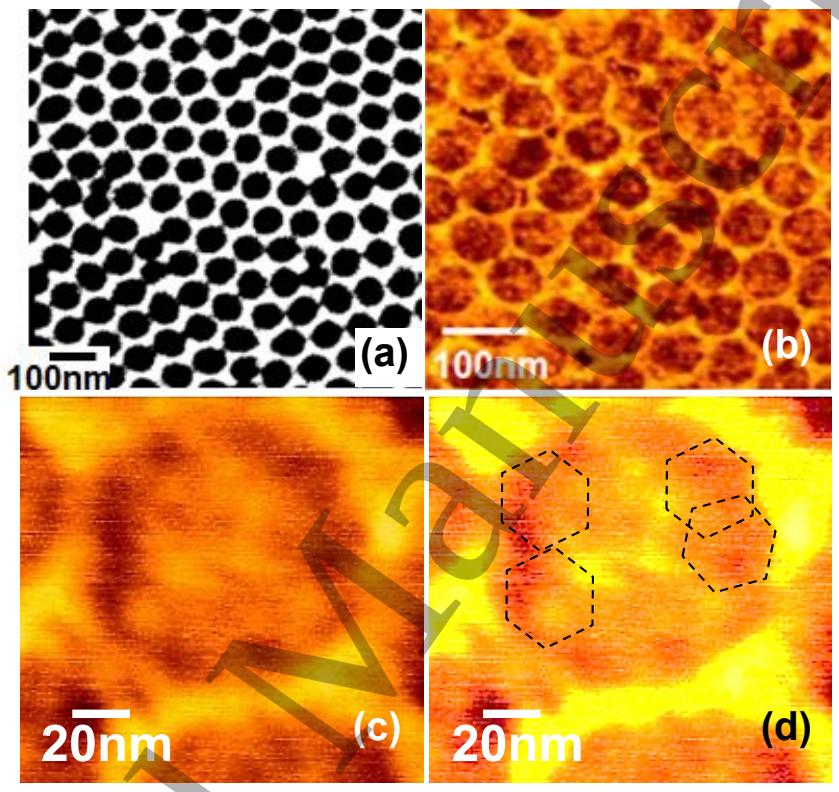

Figure 3. Examples of **(a)** SEM image of an NPAT mask and **(b)** a planer atomic force microscope image of an FGT nanomesh fabricated using (a). **(c)** Higher-resolution image of one pore in (b) and **(d)** its high-contrast image. Dotted hexagons in (d) are just to guide to eyes to confirm the angle ~ 120° of the pore edges.

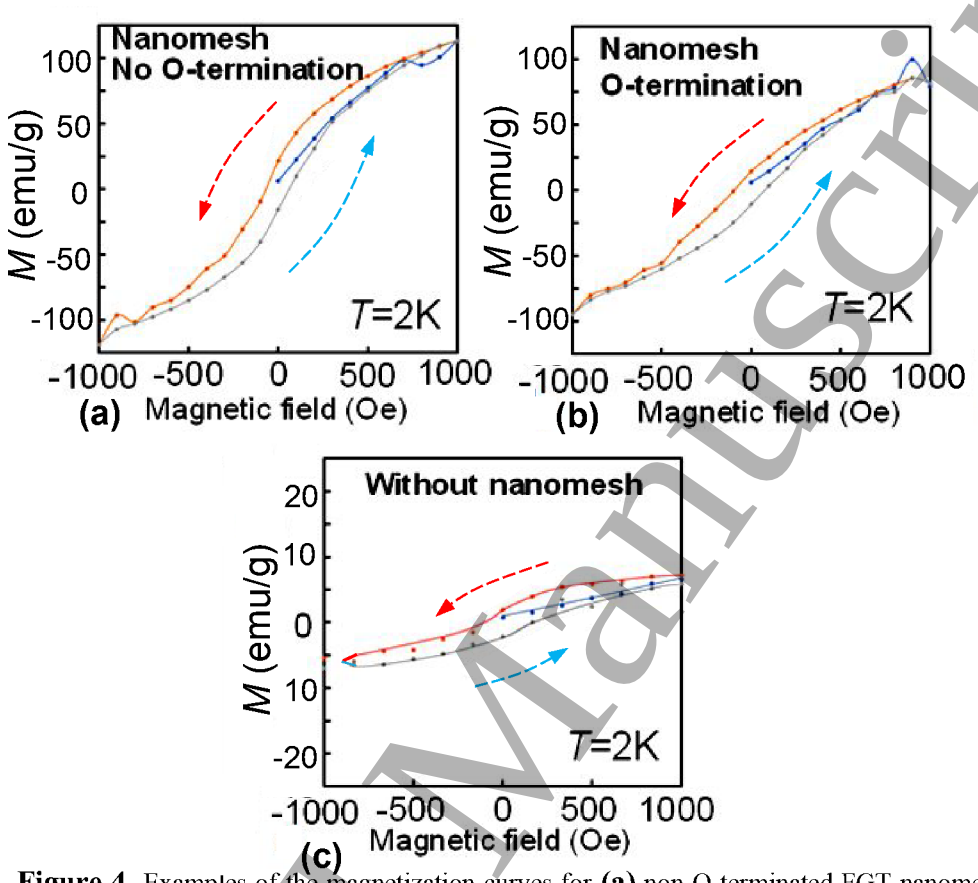

Figure 4. Examples of the magnetization curves for **(a)** non-O-terminated FGT-nanomesh(NM), **(b)** O-terminated FGT-NM, and **(c)** exfoliated pristine thin bulk flake. For (a) and (b), interpore distance (d) is ~20 nm and annealing temperature (T_a) is 700 °C. Magnetic field was applied along the c-axis (figure 1(b)) (*i.e.*, longitudinal direction of the nanopores).

	M_s (emu/g)	M_r (emu/g)	Coercivity (Oe)
Thin bulk	~7	~2	~600
O-NM	~70	~20	~1000
Non-O-NM	~120	~25	~1000

Table 1. Magnetization values and coercivity for each sample obtained from figure 4.

	O-NM	Ref.8	Ref.9	Ref.10	Ref.11	Ref.12
$M_{s//c}$ (emu/g)	~70	~20	~4	~10	~16	~1.5
$M_{s\perp c}$ (emu/g)	-	~1	~0.1	~1	~1.6	~0.5

Table 2. M_s values compared with previous reports, refs 8-12. $M_{s//c}$ and $M_{s\perp c}$ are the saturation magnetization for magnetic fields applied along and perpendicular to the c axis (figures 1(b) and 1(a)), respectively.

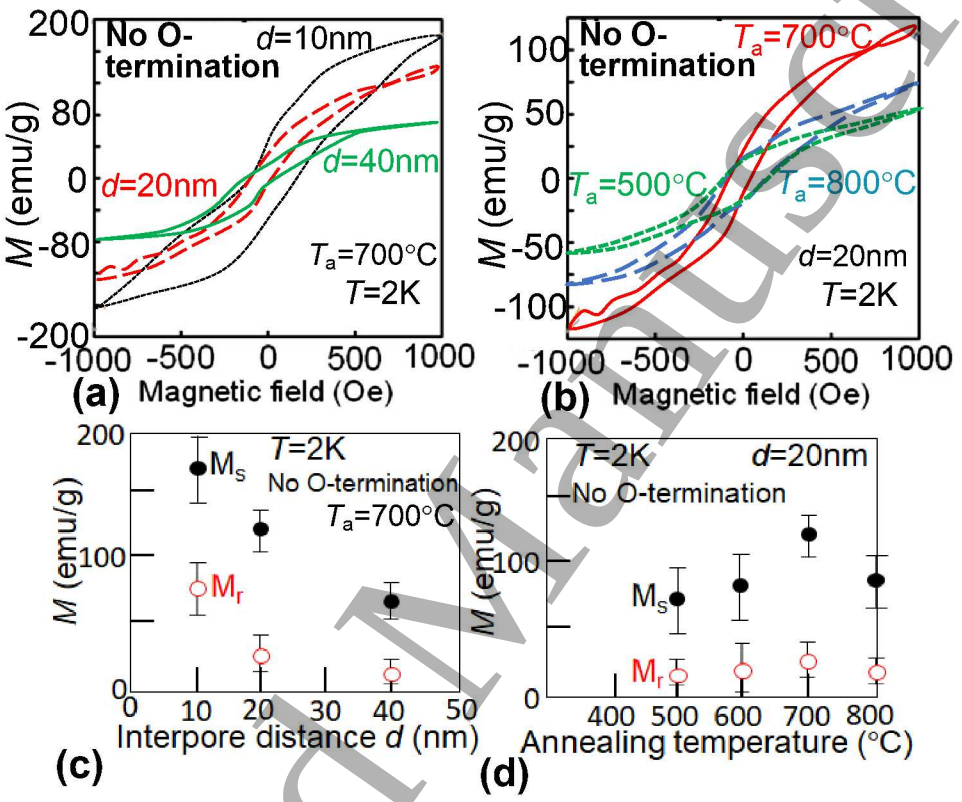

Figure 5. Magnetization curves for three different **(a)** mean interpore distance (d) and **(b)** annealing temperature (T_a) for non-O-terminated FGT nanomeshes. For (a), black- and red-dotted, and green-solid curves correspond to d ~10, 20, and 40 nm, respectively. For (b), blue- and green-dotted, and red-solid curves correspond to T_a ~800, 500, and 700 °C, respectively. Dependence of M_s and M_r values on **(c)** d obtained from (a) and **(d)** T_a obtained from (b) for non-O-terminated FGT nanomeshes.

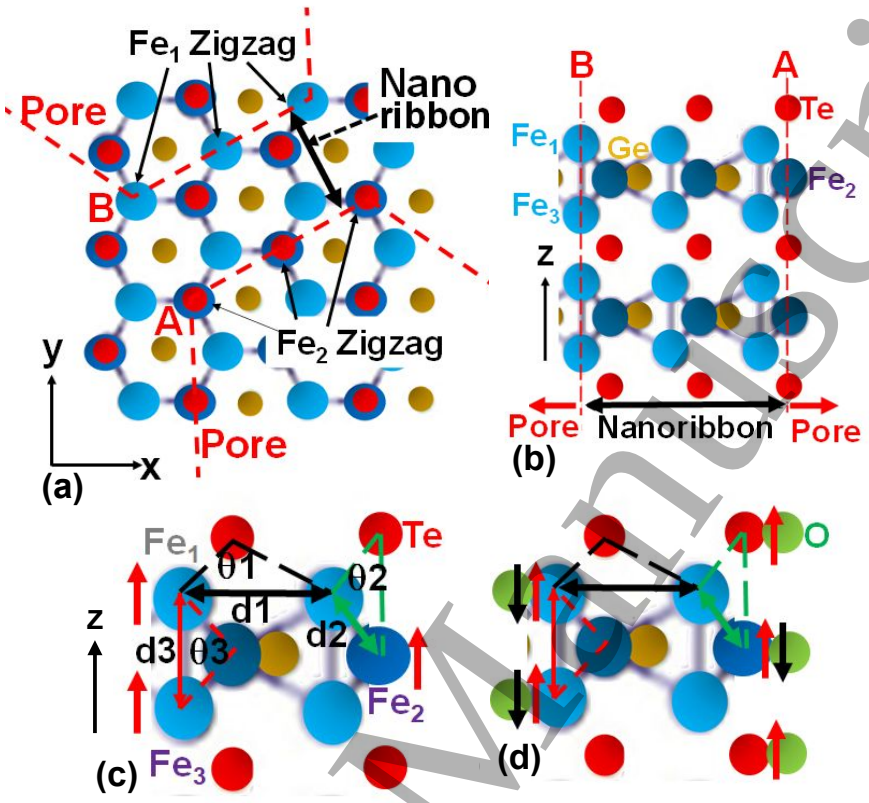

Figure 6. Schematic views for **(a)** planer and **(b)** z-direction atomic structures of an FGT nanomesh. The sections delineated by the red dotted lines and depicted as pores (part of a hexagonal-shaped pore) have no atoms in actual nanomeshes. They have been shown just for better understanding of the lattice structure. The interpore regions correspond to nanoribbon with two distinct types of zigzag edge atomic structures (*i.e.*, Fe_1 and F_3 atoms at the dangling bonds (B) and Fe_2 atoms at the dangling bonds (A). Schematic views of **(c)** the distance d_s and the angles θ among between atom sites for the non-O FGT nanomesh with FM spin alignment (red arrows) at $Fe_{1\text{-}3}$ dangling bonds (for interpretation of figure 4(a)) and **(d)** the O-FGT nanomesh with AFM spin alignment at $Fe_{1\text{-}3}$ dangling bonds coupled with O atoms (red and black arrows) (for interpretation of figure 4(b)).